Effect of nonlinearity on the steady motion of a twinning dislocation

Anna Vainchtein*

Department of Mathematics, University of Pittsburgh, Pittsburgh, PA 15260

(Dated: September 7, 2009)

Abstract

We consider the steady motion of a twinning dislocation in a Frenkel-Kontorova lattice with double-well substrate potential that has a non-degenerate spinodal region. Semi-analytical traveling wave solutions are constructed for the piecewise quadratic potential, and their stability and further effects of nonlinearity are investigated numerically. We show that the width of the spinodal region and nonlinearity of the potential have a significant effect on dislocation kinetics, reducing the velocity gaps where there is no steady motion and lowering the propagation stress. We also conjecture that a stable steady propagation must correspond to an increasing portion of the kinetic relation between the applied stress and dislocation velocity.

PACS numbers: 64.70.K-, 63.90.+t, 61.72.Bb

I. INTRODUCTION

Martensites can accommodate very large deformations (up to 10% strain in ferromagnetic shape memory alloys) due to the phenomenon of twinning.[1] A planar twin boundary separates two symmetry-related variants of the same crystalline phase. When external loading is applied, the atoms on one side of the twin boundary undergo a shear deformation relative to the other. On the microscopic level, a twin boundary propagates via the motion of twinning dislocations (also known as steps or ledges) along the boundary.[2–4] Lattice dynamics of a twinning dislocation thus largely determines the macroscopic kinetics of a twin boundary.[5]

Since the mid-sixties, a lot of progress has been made in understanding dislocation dynamics on the lattice level (see Refs. 5–12 and references therein, as well as Refs. 13, 14 and other related work reviewed in Ref. 15). Nevertheless, a number of questions remain open. In particular, existing lattice models generally predict that a dislocation cannot propagate steadily through an underdamped lattice with a velocity below a certain threshold. However, the influence of the nonlinearity of the elastic interactions on this threshold and on the existence and size of other "forbidden" velocity intervals is not well understood. It is the focus of this work.

To model the motion of a twinning dislocation, we use a variant of the well-known Frenkel-Kontorova (FK) model.[16] The model was originally formulated for slip dislocations in crystals but its various modifications have since been used to model a whole spectrum of physical and biological phenomena, including twinning, dry friction, surface reconstruction, proton conductivity of hydrogen-bonded chains, the motion of domain walls in ferroelectrics, Josephson junctions and DNA dynamics and denaturation.[15] The model consists of a linearly elastic chain of particles placed in a nonlinear substrate potential. The linear nearest-neighbor interactions model interatomic interactions on the twin plane, and the nonlinear substrate potential accounts for the interactions with other atoms. In general, the substrate potential is periodic, with alternating slip and twinning energy barriers, but since in martensitic materials such as Cu-Al-Ni the energy barriers for slip are much higher than those for twinning,[5] it suffices to consider a double-well potential. The wells correspond to two different variants of the martensite phase. A twinning dislocation is represented by a displacement profile that connects equilibrium states in two different wells. Under a force (representing an external loading of the crystal) applied to each particle, the dislocation is either pinned or

propagates through the lattice. No internal damping is introduced, so the discrete system is Hamiltonian. Although the FK model is one-dimensional, it successfully captures the essential features of the dislocation dynamics and is more transparent than its higher-dimensional counterparts.

A steadily moving dislocation is a traveling wave solution of the governing equations. As first shown in Ref. 6, exact analytical solution can be found for a two-parabola (biquadratic) substrate potential. In this case the nonlinearity is concentrated at one point where the two convex parabolae meet, and the traveling wave equation can be solved using Fourier transform. For smoother potentials, the existing literature mostly relies on the results of numerical simulations and continuum and active point approximations that are valid only within certain velocity intervals and parameter regimes.[11,17] In this paper we consider a three-parabola substrate potential where the two convex parabolas (variant wells) are connected by a concave parabola that represents a non-degenerate spinodal region. Using the approach described in Ref. 12 in the context of a high-velocity screw dislocation motion, we find the traveling wave solution at a given velocity as a convolution of a certain shape function and the already available exact solution of the problem with a biquadratic potential. The shape function can be found by solving the eigenvalue problem for an integral operator whose kernel is again determined by the solution of the two-parabola problem. Recently this approach was used to analyze the role of spinodal region in a related quasilinear problem for a phase-transforming nonlinear chain.[18] In the context of FK model, some elements of this solution procedure were first introduced in Ref. 10, but the shape functions were only found using the continuum approximation and did not in general satisfy the consistency conditions of the discrete problem.[12]

Using the constructed traveling wave profiles, we study the influence of the width of the spinodal region on the kinetic relation between the applied stress and the dislocation velocity. We find that a sufficiently wide spinodal region substantially changes the kinetics of a twinning dislocation. As in Refs. 18 and 12, the obtained solutions feature smaller amplitude of the lattice waves emitted by the moving front and a smaller driving force. This results in the existence of small-velocity solutions with lattice waves of different wave lengths emitted both ahead and behind the moving dislocation. The velocity intervals containing such solutions are separated by *velocity gaps* where no traveling wave solutions exist. These gaps become narrower, and the lowest propagation speed becomes smaller, as the width

of the spinodal region is increased. In contrast, in the biquadratic case (or when spinodal region is narrow enough) traveling wave solutions exist only at relatively large velocities and have a single oscillation mode propagating behind the dislocation.[6] The only velocity gap in this case is between the zero speed and the lowest propagation speed.

To verify the obtained solutions and study their stability, we conduct a series of numerical simulations of the initial value problem for the original discrete system. We use either piecewise constant displacement or the constructed solutions as initial conditions. As in numerical simulations in Refs. 17, 10 (which include damping), we see that the dislocation does not propagate until the applied stress reaches a certain threshold value σ_T. This value is lower than the Peierls stress σ_P below which equilibrium states exist and are locally stable. Above σ_T the numerical solution around the front converges to one of the constructed traveling waves, suggesting its stability. Since the numerical simulations only fall onto the increasing portions of the kinetic curve, we conjecture that this is a necessary (but not sufficient) condition for stability of steady dislocation motion. In the biquadratic case this is consistent with the hypothesis in Ref. 6 that only traveling waves above the minimum stress (called dynamic Peierls stress) of the highest-velocity kinetic segment are stable. As the width of the spinodal region is increased, the speed of the first stable traveling wave decreases. When the spinodal region is wide enough, there are two or more stable segments of the kinetic relation that correspond to different number of radiative modes emitted by the moving front. These segments are separated by velocity intervals where there is no stable steady propagation.

To access the effect of full nonlinearity, we consider a one-parameter family of smooth functions that approximate the three-parabola potential at small values of the parameter. Numerical simulations with these potentials show that velocity gaps persist. Thus the gaps are not an artifact of piecewise quadratic potentials but rather a generic feature of the discrete model. At large parameter value (strong nonlinearity) the lowest propagation speed becomes notably smaller, reducing, but not eliminating, the first velocity gap. This indicates that the nonlinearity itself, and not only the width of the spinodal region, determines the lowest propagation speed.

Overall, we find that nonlinearity in general and a sufficiently wide spinodal region in particular reveal a more complex structure of stable solutions of the FK model than the one suggested by the biquadratic model. In particular, we show that a twinning dislocation can

move steadily at speeds that are "forbidden" in the biquadratic case and emit waves in both directions. The combination of semi-analytical calculations and numerical simulations allows us to see features of the discrete kinetics, such as velocity gaps and the detailed structure of emitted lattice waves, that are easy to miss if one relies on numerical simulations alone.

The rest of the paper is organized as follows. The model is introduced in Sec. II, and the traveling wave solutions for the three-parabola potential are constructed in Sec. III. In Sec. IV we discuss solution admissibility, obtain the kinetic relation and analyze their dependence on the width of the spinodal region. The equilibrium states are discussed in Sec. V. In Sec. VI we present the numerical simulations that suggest stability of some of the obtained solutions. The effect of nonlinearity is further analyzed in Sec. VII, and the concluding remarks can be found in Sec. VIII.

II. THE MODEL

Consider an infinite Frenkel-Kontorova chain of particles of mass m connected by massless linear springs to each other and interacting with an external substrate potential $\Phi(u_n)$, where $u_n(t)$ is the displacement of nth mass from its reference position at time t. We assume that the particles can move only along one direction and that an external stress σ, acting in the same direction, is applied to each mass. Let ε denote the reference length of the linear springs and $\rho = m/\varepsilon$ be the mass denisty. The total energy of the system is given by

$$\mathcal{E} = \sum_{n=-\infty}^{\infty} \left[\frac{1}{2}\rho\varepsilon\dot{u}_n^2 + \frac{1}{2}E\varepsilon\left(\frac{u_{n+1}-u_n}{\varepsilon}\right)^2 + \varepsilon(\Phi(u_n) - \sigma u_n) \right],$$

and the equations of motion are

$$\rho\varepsilon\ddot{u}_n - \frac{E}{\varepsilon}(u_{n+1} - 2u_n + u_{n-1}) + \varepsilon(\Phi'(u_n) - \sigma) = 0.$$

Here $\dot{u}_n$ and $\ddot{u}_n$ denote the first and second derivatives of $u_n(t)$, respectively, and $E > 0$ is the elastic modulus of the harmonic nearest-neighbor interactions. To model twinning, we assume that the substrate potential has two symmetric wells that represent two different variants of the martensite phase. The wells are located at $u = \pm a$ and have the local elastic modulus G:

$$\Phi'(\pm a) = 0, \quad G = \Phi''(\pm a) > 0.$$

We now introduce the dimensionless variables

$$\bar{t} = \frac{t}{\varepsilon}\sqrt{\frac{\rho}{E}}, \quad \bar{u}_n = \frac{u_n}{a}, \quad \bar{\sigma} = \frac{\sigma}{aE}, \quad \bar{\Phi} = \frac{\Phi}{aE} \tag{1}$$

and the dimensionless parameter

$$\mu = \frac{G\varepsilon^2}{E} \tag{2}$$

measuring the relative stiffness of the nonlinear interaction with the substrate. In terms of the new variables, with the bars dropped, the dimensionless equations of motion are

$$\ddot{u}_n = u_{n+1} - 2u_n + u_{n-1} + \mu(\sigma - \Phi'(u_n)). \tag{3}$$

To obtain semi-analytical results, we will further assume that the substrate potential is piecewise quadratic, with a continuous piecewise linear derivative

$$\Phi'(u) = \begin{cases} u + 1, & u < -\delta/2 \\ (1 - 2/\delta)u, & -\delta/2 \le u \le \delta/2 \\ u - 1, & u > \delta/2, \end{cases} \tag{4}$$

The two linearly increasing segments correspond to the two symmetric quadratic wells of $\Phi(u)$, connected by a downward parabola ($|u| < \delta/2$) that represents the *spinodal region* of width δ such that

$$0 \le \delta < 2.$$

III. TRAVELING WAVE SOLUTIONS

To model a steadily moving twinning dislocation, we seek solutions of (3) in the form of a traveling wave:

$$u_n = u(\xi), \quad \xi = n - Vt. \tag{5}$$

Substituting this ansatz in (3), we obtain the advance-delay differential equation

$$V^2 u'' = u(\xi + 1) - 2u(\xi) + u(\xi - 1) + \mu(\sigma - \Phi'(u(\xi))). \tag{6}$$

In what follows, we will assume that $\Phi'(u)$ is given by (4). We are interested in finding solutions of (6) subject to the following conditions at infinity:

$$\langle u(\xi) \rangle \to \sigma \mp 1 \quad \text{as } \xi \to \pm\infty. \tag{7}$$

Here $\sigma \mp 1$ are stable equilibrium solutions of (6), and the angular brackets denote the average value of the displacement because we expect the Hamiltonian discrete system to develop oscillations. The average is taken over the largest oscillation period.

To solve the problem (6), (7) for given $V > 0$ and find the corresponding $\sigma = \sigma(V)$, we follow the approach of Ref. 12, recently applied to a related quasilinear problem in Ref. 18. Since the details of the solution procedure can be found in Refs. 12 and 18, we only outline the main steps. First, we assume that $u(\xi)$ takes values inside the spinodal region ($|u| < \delta/2$) when ξ is in the interval $|\xi| < z$, for some $z > 0$ to be determined. We further assume that for $\xi < -z$ we have $u > \delta/2$ (second well) and for $\xi > z$ we have $u < \delta/2$ (first well). Then we can write

$$\Phi'(u(\xi)) = u(\xi) - \int_{-z}^{z} h(s)(2\theta(s) - 1)ds, \tag{8}$$

where $\theta(s)$ is a unit step function, and we introduced an unknown shape function $h(s)$ which is zero outside the interval $[-z, z]$ and is normalized so that

$$\int_{-z}^{z} h(s)ds = 1 \tag{9}$$

Thus we obtain

$$V^2 u'' + (\mu + 2)u(\xi) - u(\xi + 1) - u(\xi - 1) = \mu(\sigma - 1 + 2\int_{-z}^{z} h(s)\theta(s - \xi)ds). \tag{10}$$

For consistency, we must require that in addition to (10) and (7), the solution satisfies the conditions

$$u(z) = -\frac{\delta}{2}, \quad u(-z) = \frac{\delta}{2} \tag{11}$$

and the inequalities

$$\begin{aligned} u(\xi) &> \frac{\delta}{2}, \quad \xi < -z \\ |u(\xi)| &< \frac{\delta}{2}, \quad |\xi| < z \\ u(\xi) &< -\frac{\delta}{2}, \quad \xi > z \end{aligned} \tag{12}$$

Applying Fourier transform to (10) and using the convolution theorem, one can show (see Ref. 18 for details) that

$$\frac{du}{d\xi} = -\int_{-z}^{z} h(s)q(\xi - s)ds, \tag{13}$$

where the kernel is the negative derivative of the solution $u^0(\xi)$ of the problem with biquadratic potential with a degenerate spinodal region ($\delta = 0$):

$$q(\xi) = -\frac{du^0}{d\xi}. \tag{14}$$

At the same time, (4) and (8) imply that for $|\xi| < z$

$$\frac{d}{d\xi}\Phi'(u(\xi)) = \left(1 - \frac{2}{\delta}\right)u'(\xi) = u'(\xi) + 2h(\xi),$$

and thus $u'(\xi) = -\delta h(\xi)$ for $|\xi| < z$. Together with (13), this yields the integral equation

$$\int_{-z}^{z} h(s)q(\xi - s)ds = \delta h(\xi), \quad |\xi| < z. \tag{15}$$

Thus the shape function $h(\xi)$ is the eigenfunction of the integral operator in the left hand side of (15) with the kernel (14) associated with the eigenvalue δ. The eigenvalue problem is similar to the the ones obtained in Ref. 12 for the uniform motion of a screw dislocation and in Ref. 18 for the motion of a phase boundary (with different kernels) and was derived in the same way.

The solution for any nonzero δ is thus obtained from the solution $u^0(\xi)$ for the case of $\delta = 0$ (biquadratic potential). The latter can be found exactly using Fourier transform[6] (see also Refs. 17, 11 for more details). Performing these calculations for our case, we obtain

$$u^0(\xi) = \begin{cases} \sigma^0 - 1 - 2\mu \sum\limits_{k \in M^+(V)} \dfrac{e^{ik\xi}}{kL_k(k,V)}, & \xi > 0 \\ \sigma^0 + 1 + 2\mu \sum\limits_{k \in M^-(V)} \dfrac{e^{ik\xi}}{kL_k(k,V)}, & \xi < 0, \end{cases} \tag{16}$$

where

$$\sigma^0 = 2\mu \sum_{k \in N(V)} \frac{1}{|kL_k(k,V)|}. \tag{17}$$

Here

$$M^{\pm}(V) = \{k : L(k,V) = 0,\ \mathrm{Im}k \gtrless 0\} \bigcup N^{\pm}(V) \tag{18}$$

are all roots of the dispersion relation

$$L(k,V) = \mu + 4\sin^2\frac{k}{2} - V^2k^2 \tag{19}$$

contributing to the solution on either side of the front, and

$$N^{\pm}(V) = \{k : L(k,V) = 0,\ \mathrm{Im}k = 0,\ kL_k(k,V) \gtrless 0\} \tag{20}$$

denotes the sets of real roots distributed according to the radiation condition[6,11]. Note that the applied stress σ^0 in (17) is determined entirely by the real roots, which correspond to phonon waves that carry energy away from the moving front (radiative damping). As shown in Ref. 11, one can derive (17) by accounting for the energy fluxes carried by these waves.

Knowing the solution for $\delta = 0$ and a given $V > 0$, we determine the kernel of the integral operator in (15),

$$q(\xi) = \begin{cases} 2\mu i \sum\limits_{k \in M^+(V)} \dfrac{e^{ik\xi}}{L_k(k,V)}, & \xi > 0 \\ -2\mu i \sum\limits_{k \in M^-(V)} \dfrac{e^{ik\xi}}{L_k(k,V)}, & \xi < 0, \end{cases} \tag{21}$$

and find the unknown shape function $h(\xi)$ and its support $[-z, z]$ using a numerical approximation of (15), as described in the next section. The solution for $\delta > 0$ is then given by

$$u(\xi) = \sigma - \sigma^0 + \int_{-z}^{z} h(s) u^0(\xi - s) ds, \tag{22}$$

where the applied stress

$$\sigma = \sigma^0 - \frac{1}{2} \int_{-z}^{z} h(s)(u^0(z - s) + u^0(-z - s)) ds \tag{23}$$

is found by using the switch conditions (11).

IV. ADMISSIBLE SOLUTIONS AND KINETIC RELATIONS

Since solutions of the problem with biquadratic substrate potential ($\delta = 0$) serve as the foundation for the construction of the traveling wave solutions in the case of a non-degenerate spinodal region, we start by briefly reviewing their properties. The reader is referred to Refs. 6, 17, 11 for additional details.

For each non-resonant velocity $V > 0$, one can calculate the traveling wave solution (16) and compute the corresponding applied stress σ using (17). The resulting functional relation $\sigma = \sigma(V)$, often referred to as a *kinetic relation*, is shown in Figure 1 for the case of $\mu = 1$. The relation consists of disjoint segments separated by *resonance velocities*, i.e. values of V such that $L(k, V) = 0$ and $L_k(k, V) = 0$ for some real k. A typical solution above the first resonance ($V = 0.5$) is shown in grey in Figure 2. One can see that a moving dislocation emits phonon oscillations behind it, with the wave number corresponding to the single real root of (19). As velocity decreases below the first resonance (see the grey curve at $V = 0.2$ in

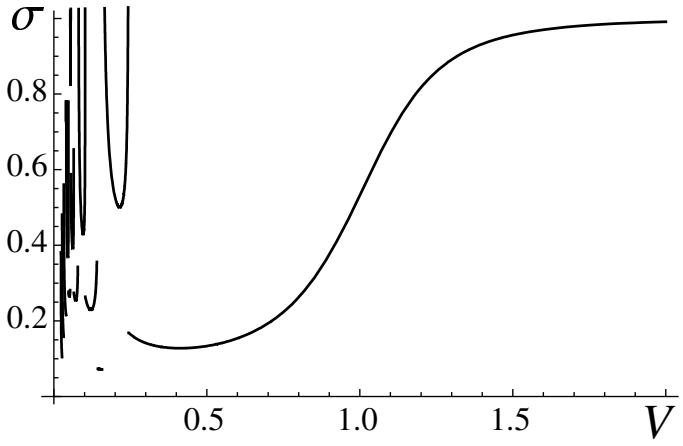

FIG. 1: Kinetic relation in the case of the biquadratic potential ($\delta = 0$). Only a few segments are shown at low velocities. Here $\mu = 1$.

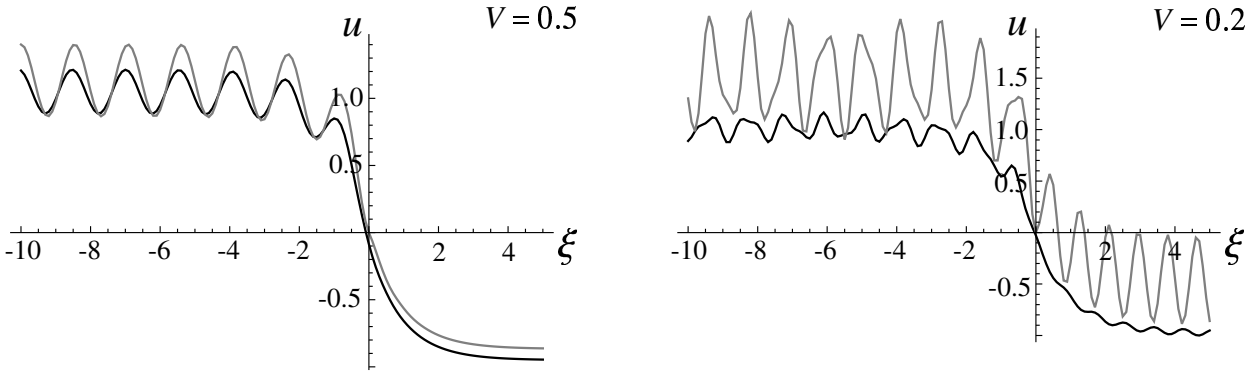

FIG. 2: Displacement profiles at $\delta = 0$ (grey curves) and $\delta = 0.8$ (black). At $\delta = 0$ the traveling wave solution at $V = 0.5$ is admissible, while the one at $V = 0.2$ is not. At $\delta = 0.8$ both solutions are admissible. Here $\mu = 1$.

Figure 2), more oscillation modes appear, and the formally obtained $u^0(\xi)$ features phonon emission on both sides. However, a closer inspection reveals that this "solution" is in fact inadmissible and should be removed because it violates the assumption that $u^0(\xi) < 0$ for $\xi > 0$. In fact, all segments of the kinetic relation below the first resonance do not contain any admissible traveling waves and thus need to be removed, while the remaining large-velocity segment contains admissible solutions above a certain threshold velocity[11] (in the case of $\mu = 1$, $V \geq 0.35$). This implies non-existence of traveling wave solutions with the velocity lower than the threshold value in the $\delta = 0$ case. Nevertheless, as we will see, some

of the solutions that are non-admissible in this case still play an important role because they are used to construct admissible low-velocity solutions when the spinodal region is no longer degenerate.

Consider now potentials with nonzero δ. The procedure used to find the traveling wave solutions and obtain the kinetic relations in this case is as follows. After computing the kernel (14) of the integral operator in (15) from the solution for $\delta = 0$ case for given V, the integral equation is approximated using the trapesoidal rule for a finite z, so that the eigenvalue problem reduces to finding z and $\mathbf{h}$ such that the given δ is an eigenvalue of the resulting matrix in the numerical approximation, and the vector $\mathbf{h}$ is the corresponding eigenvector that approximates the eigenfunction $h(\xi)$. In some cases, there are two values of z but our calculations show that at most one value yields admissible solutions that satisfy the constraints (12). Once z and $\mathbf{h}$ are found, the trapesoidal approximation of the integrals in (22) and (23) is used to compute the solution $u(\xi)$ and the applied stress σ.

The resulting displacement profiles at $\delta = 0.8$ are shown by black curves in Figure 2. The main effects of $\delta > 0$ are the phase shift, the decreased amplitude of the oscillations and the lower value of the applied stress. These were also observed and explained in Ref. 12. The phase shift occurs due to the continuous particle acceleration at $\delta > 0$ (as opposed to the discontinuity at $t = n/V$ when $\delta = 0$), which results in lower velocities and thus longer time needed to reach the maxima of oscillations. Meanwhile, wave modulation during the finite time interval $[n - z/V, n + z/V]$ when $\Phi'(u_n)$ for the well-switching nth particle has the negative slope leads to the diminished contribution of the short-wave oscillations to the energy radiation (and thus lower applied stress).

As a result of the smaller wave amplitude, some velocities for which solutions were inadmissible at $\delta = 0$ may in fact lead to admissible solutions at sufficiently large nonzero δ. For example, the solution at $V = 0.2$ is admissible at $\delta = 0.8$, while the corresponding solution for the biquadratic potential is not. Thus, as in Ref. 18, we conclude that the main feature of the dynamics with a smoother substrate potential is the existence of traveling waves at least at some small velocities away from the resonances.

Figure 3(a) shows the half-width z of the transition region as the function of V for $\delta = 0.4$, 0.8 and 1.2. One can see that z increases with δ, as expected. Note also that along the highest-velocity segment (above the first resonance) z initially decreases as V grows (more rapidly at larger δ), reaches a minimum at a moderately large velocity and then increases.

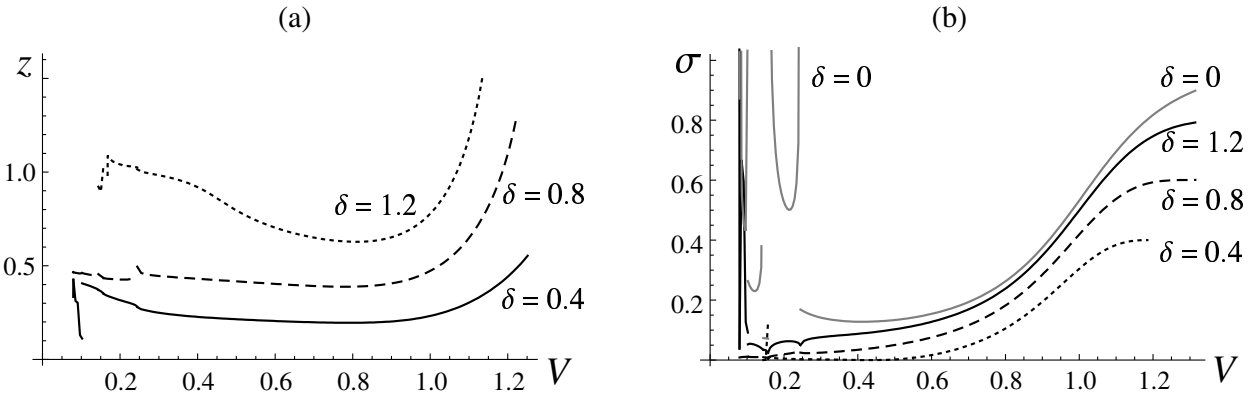

FIG. 3: (a) The half-width z of the transition region as the function of V for different δ. (b) The corresponding kinetic relations, shown together with the one for $\delta = 0$. Only a few segments are shown at low velocities. Here $\mu = 1$.

The corresponding kinetic relations, along with the one for $\delta = 0$ (in grey) are shown in Figure 3b. Note that resonances, while still present, become much less pronounced as δ increases, while the applied stress decreases at each V. As remarked above, some velocity intervals around the resonances need to be removed for each δ (and the entire low-velocity interval below a certain speed needs to be removed when $\delta = 0$) because they do not contain admissible traveling waves. These intervals get smaller as δ increases and more low-velocity solutions become admissible.

As V tends to infinity, the kinetic relation approaches the spinodal value $\sigma_S = 1 - \delta$, the maximum value for which there exist equilibrium solutions of $\Phi'(u) = \sigma$ in two different wells. We remark that at sufficiently large velocities ($V > 1$) the amplitude of the waves propagating behind becomes so large that the oscillations enter the spinodal region, violating the constraint $u(\xi) > \delta/2$ at $\xi < -z$ that was assumed to obtain solutions. The corresponding solutions are thus technically not admissible, although, as we will see, they are still very close to the displacement profiles obtained numerically.

V. LATTICE TRAPPING AND THE PEIERLS THRESHOLD.

In addition to dynamic solutions, there are trapped equilibrium states ($V = 0$) governed by the system of difference equations

$$u_{n+1} - 2u_n + u_{n-1} + \mu(\sigma - \Phi'(u_n)) = 0 \tag{24}$$

Solutions of (24) can be found, for example, in Ref. 19. Here we merely summarize the results for completeness using our notation.

If no particles have displacement in the spinodal region, the problem is solved the same way as in the case of biquadratic potential considered in Ref. 20. The equilibrium solutions with a single dislocation that has larger displacement behind are given by

$$u_n = \begin{cases} \sigma - 1 + Ay_2^n, & n \geq 0 \\ \sigma + 1 + (A-2)y_1^n, & n < 0, \end{cases} \tag{25}$$

with

$$A = \frac{\sqrt{4+\mu} - \sqrt{\mu}}{\sqrt{4+\mu}}$$

and

$$y_{1,2} = 1 + \frac{\mu}{2} \pm \frac{\sqrt{\mu}}{2}\sqrt{4+\mu}.$$

Solutions (25) exist if and only if the applied stress is inside the *trapping region* $|\sigma| \leq \sigma_P$, where

$$\sigma_P = \frac{\sqrt{\mu}}{\sqrt{4+\mu}} - \frac{\delta}{2} \tag{26}$$

is the *Peierls stress*. At stresses outside the trapping region only dynamic solutions exist. Since the Peierls stress must be nonnegative, the obtained equilibrium solutions only exist for suffficiently narrow spinodal regions, i.e. when

$$0 \leq \delta \leq \frac{2\sqrt{\mu}}{\sqrt{4+\mu}}.$$

For larger δ, equilibria must have at least one particle with spinodal displacement. The trapped states in the case of a single particle in the spinodal region are again given by (25) but with

$$A = 1 + \frac{2\mu\sigma y_1}{\delta((2+\mu)y_1 - 2) - 2\mu y_1},$$

and the Peierls stress becomes

$$\sigma_P = \frac{(1 - y_2 - \delta/2)(\delta((2+\mu)y_1 - 2) - 2\mu y_1)}{2\mu(1-y_1) + \delta((2+\mu)y_1 - 2)}. \tag{27}$$

Notice that the dependence on δ is no longer linear, as it was for (26). These solutions exist whenever

$$\frac{2\sqrt{\mu}}{\sqrt{4+\mu}} \leq \delta \leq \sqrt{\mu}(\sqrt{4+\mu} - \sqrt{\mu}).$$

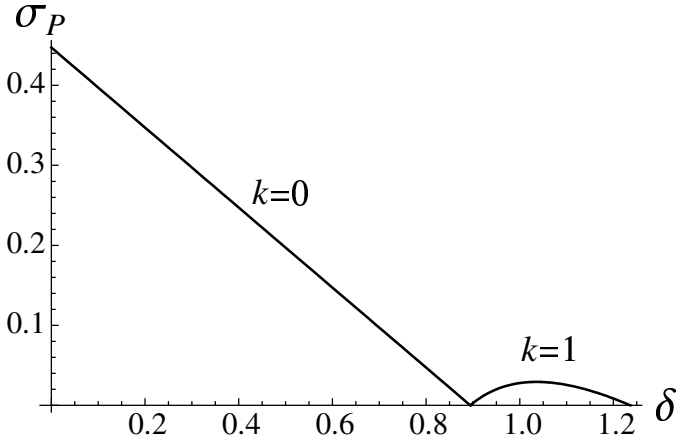

FIG. 4: Dependence of the Peierls stress on the width δ of the spinodal region at $\mu = 1$. Here k denotes the number of particles in the spinodal region in the corresponding trapped equilibria.

Figure 4 shows the dependence of Peierls stress on the width δ of the spinodal region for the cases of zero and one spinodal particles. Note that there is no lattice trapping ($\sigma_P = 0$) at $\delta = 2\sqrt{\mu}/\sqrt{4+\mu}$ and $\delta = \sqrt{\mu}(\sqrt{4+\mu} - \sqrt{\mu})$. At $\delta > \sqrt{\mu}(\sqrt{4+\mu} - \sqrt{\mu})$ we need to insert two particles in the spinodal region, then three, etc.

VI. STABILITY OF THE TRAVELING WAVES: NUMERICAL SIMULATIONS

To access stability of the obtained traveling waves and verify the above calculations, we conducted a series of numerical simulations of the Riemann initial value problem with the initial displacement

$$u_n(0) = \begin{cases} \sigma + 1, & n < n_0 \\ s, & n = n_0 \\ \sigma - 1, & n > n_0, \end{cases} \tag{28}$$

where $0 \le s \le \delta/2$, and zero initial velocity. For a given applied stress σ, we solved the system (3) of ordinary differential equation for a truncated lattice with N masses (typically $N = 600$ but a longer chain is used if the simulation runs for a long time, in order to avoid reflection of elastic waves from the domain boundaries), subject to the above initial conditions and the corresponding boundary conditions. After a sufficiently long time (usually $t = 200$ but longer for small-velocity solutions), the solution aproaches an attractor corresponding to either a stationary dislocation (zero velocity) or a periodic front motion with a steady

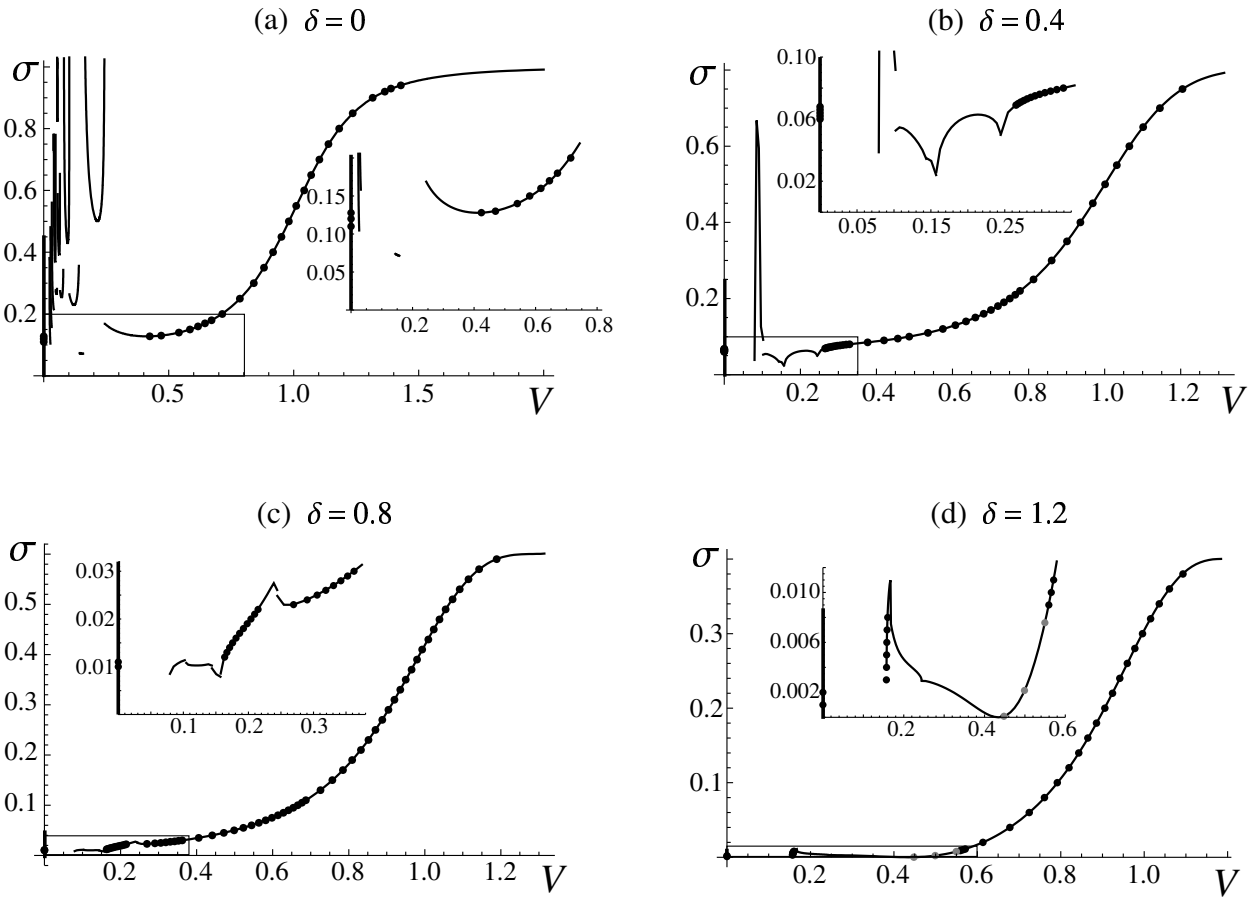

FIG. 5: Results of the numerical simulations (black dots) with initial displacement (28) and zero initial velocity, shown together with the kinetic curves for (a) $\delta = 0$, (b) $\delta = 0.4$, (c) $\delta = 0.8$ and (d) $\delta = 1.2$. Here $\mu = 1$ and in (28) $s = 0$ in (a) and $s = 0.1$ in (b-d). The thick vertical segment along $V = 0$ axis indicates the trapping region. The grey dots in (d) are the results of the numerical simulations with the corresponding traveling wave taken as the initial condition. Inserts zoom in on the corresponding rectangles near the origin.

period T, yielding the velocity $V = 1/T$. The velocity is averaged over the last ten periods.

Figure 5 shows the results for different values of δ and compares the numerical results with the semi-analytical kinetic curves. Thick vertical segment along $V = 0$ axis indicates the trapping region $0 \le \sigma \le \sigma_P$ in each case. For sufficiently small σ the long-time solution corresponds to an equilibrium state ($V = 0$) superimposed with elastic waves propagating away from the trapped dislocation. Once σ exceeds a certain threshold value σ_T (which is below the Peierls stress σ_P), the front starts moving with a finite velocity V, and the solution around the front approaches the traveling wave solution we constructed with the

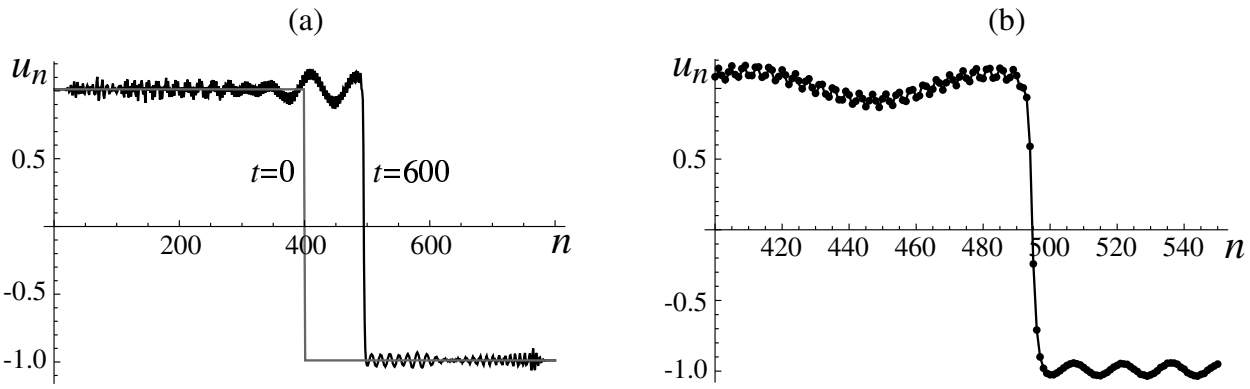

FIG. 6: (a) Displacement profiles at $t = 0$ and $t = 600$ for the numerical simulation at $\delta = 0.8$, $\mu = 1$ and $\sigma = 0.011$. (b) The numerical solution (dots) around the dislocation front compared to the traveling wave solution (solid curve) with the same velocity, $V = 0.162$.

same velocity. Note that this transition is accompanied by a finite *jump* in velocity over a very small change in the applied stress. For example, at $\delta = 0.4$, the stress $\sigma = 0.068$ yields $V = 0$ but at $\sigma = 0.069$ we obtain $V = 0.265$ (see Figure 5b). In this case and at $\delta = 0$ (Figure 5a) the jump is from zero velocity to a solution on the first (higher-velocity) segment of the kinetic relation. But at $\delta = 0.8$ (Figure 5c) and $\delta = 1.2$ (Figure 5d) the numerical solutions instead approach a traveling wave along the second kinetic segment, with velocities $V = 0.162$ ($\sigma = 0.011$) and $V = 0.157$ ($\sigma = 0.003$), respectively. See Figure 6, where the numerical solution at $\delta = 0.8$ that yields $V = 0.162$ is compared to the corresponding traveling wave solution. Recall that these solutions feature a dislocation emitting oscillations in both directions and that there are no admissible traveling waves at these velocities when $\delta = 0$. As we increase σ, the numerical results continue to follow the corresponding kinetic curves. In the case of $\delta = 0.8$ and $\delta = 1.2$ the second kinetic segments is followed for a while, and then there is another velocity jump, to the first kinetic segment. Specifically, at $\delta = 0.8$ the jump is from $V = 0.215$ at $\sigma = 0.022$ to $V = 0.269$ at $\sigma = 0.023$ (see the insert in Figure 5c). In case of $\delta = 1.2$, the jump is even bigger, from $V = 0.16$ at $\sigma = 0.008$ to $V = 0.559$ at $\sigma = 0.009$ (see the black dots in the insert in Figure 5d). However, numerical simulations with the corresponding traveling waves taken as initial conditions instead of (28) suggest stability of all solutions along the first kinetic segment starting with its minimum point, $V = 0.45$ (see the grey dots in the insert in Figure 5d). Meanwhile, solutions along the portion of the segment where σ is decreasing

appear to be unstable: for example, when the traveling wave with $V = 0.35$ is used as the initial condition, the numerical solution converges to the traveling wave with $V = 0.489$, which is located on the increasing portion of the kinetic segment at the same applied stress. In general, our simulation results suggest the following

Conjecture. *A necessary (but not sufficient) condition for stability of the traveling wave solution of* (3) *with velocity* V *is that it is located on the increasing portion of the kinetic curve:* $\sigma'(V) > 0$.

We emphasize that the above condition is not sufficient. For example, at $\delta = 0.8$ the traveling wave solution with $V = 0.24$ is admissible and located along the increasing part of the second segment of the kinetic curve (see the insert in Figure 5c). Using it as an initial condition, however, we obtain the traveling wave with $V = 0.336$, which is located along the increasing portion of the first kinetic segment. The necessity of the condition $\sigma'(V) > 0$ is suggested by the observation that each traveling wave solution obtained via the numerical simulation is located on an increasing portion of the kinetic relation. Proving this conjecture is not an easy task even in the biquadratic case where stable dynamic solutions are located only on the higher-velocity segment of the kinetic relation. In this case a proof of stability of traveling waves with sufficiently high velocities can be found in Ref. 21, along with some remarks about extending these results to smoother potentials. Unfortunately, the proof does not extend to the entire conjectured stability interval, since it relies on positivity of Green's functions, and in the conservative case these functions change sign at speeds below a certain value.[21]

As remarked above, the threshold value σ_T beyond which the dislocation is no longer static in the Riemann simulations is *below* the Peierls threshold σ_P, meaning that the initial conditions for $\sigma > \sigma_T$ are in the basin of attraction of the solutions with a moving dislocation. Nevertheless, the equilibrium states remain locally stable and coexist with the dynamic solutions for $\sigma_T < \sigma < \sigma_P$[17].

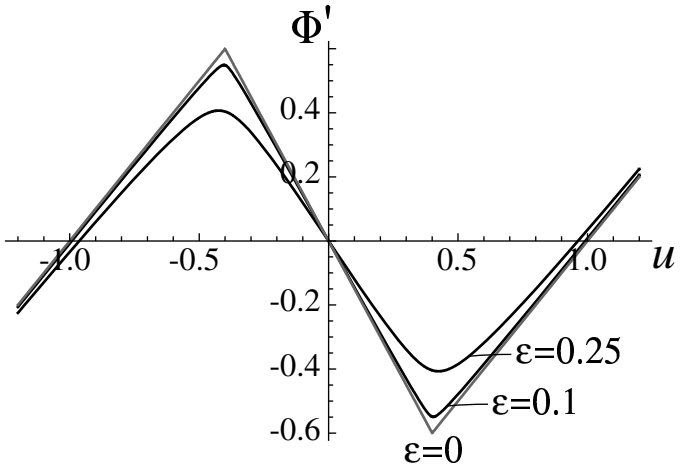

FIG. 7: The first derivative of the potential $\Phi_\varepsilon(u)$ defined in (29) for $\varepsilon = 0$ (grey curve) and $\varepsilon = 0.1$ and 0.25 (black curves). Here $\delta = 0.8$ and $\mu = 1$.

VII. FULLY NONLINEAR POTENTIALS

In order to obtain semi-analytical solutions, we have assumed that the potential $\Phi(u)$ (for $\delta > 0$) has piecewise linear continuous first derivative and piecewise quadratic discontinuous second derivative. To access the effect of full nonlinearity on the Frenkel-Kontorova kinetics, for given $\delta > 0$ we now consider a family of fully nonlinear potentials $\Phi_\varepsilon(u)$ with the second derivative given by

$$\Phi''_\varepsilon(u) = \mu\left(1 - \frac{1}{\delta} + \frac{2}{\pi\delta}\arctan\frac{u^2 - \frac{\delta^2}{4}}{\varepsilon^2}\right). \tag{29}$$

In the limit $\varepsilon \to 0$ $\Phi''_\varepsilon(u)$ approaches the piecewise constant discontinuous second derivative $\Phi''(u)$ of the potential defined by (4). At small ε $\Phi'_\varepsilon(u)$ approximates the piecewise linear function $\Phi'(u)$ by smoothing its corners; see Figure 7.

The results of the Riemann simulations using the fully nonlinear potentials with $\varepsilon = 0.1$ and $\varepsilon = 0.25$ are shown in Figure 8, where the kinetics for the piecewise linear case ($\varepsilon = 0$, grey curve) is also included for comparison. In each case we see two dynamic branches. The threshold stresses beyond which the dislocation in the solution of the Riemann problem is no longer stationary are $\sigma_T = 0.011$ for $\varepsilon = 0$, $\sigma_T = 0.0104$ for $\varepsilon = 0.1$ and $\sigma_T = 0.0001$ for $\varepsilon = 0.25$. As ε increases, the stress at each velocity decreases, which is consistent with the fact that the limiting spinodal stress also becomes lower. Observe that the velocity gaps between first and second kinetic branches are nearly identical in all three cases, showing

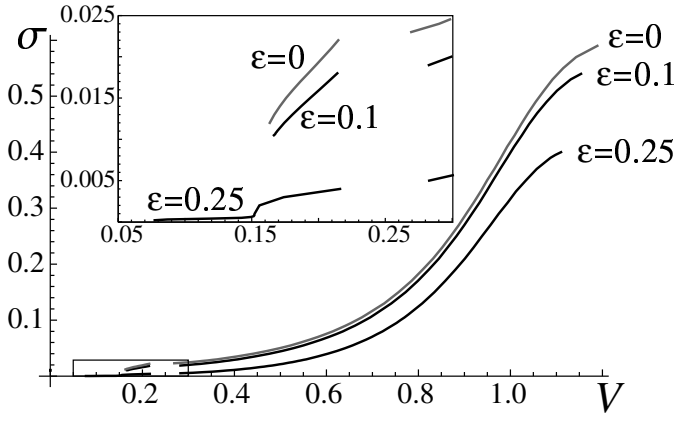

FIG. 8: Results of Riemann simulations at $\varepsilon = 0.1$ and 0.25 (black curves), shown along with the results for $\varepsilon = 0$ (in grey). Insert zooms in on the rectangle near the origin. Here $\delta = 0.8$ and $\mu = 1$.

that it is not an artifact of piecewise linearity but rather an intrinsic feature of the discrete model. Note, however, that while the lowest nonzero velocity is nearly the same for piecewise quadratic ($\varepsilon = 0$) and "almost piecewise quadratic" ($\varepsilon = 0.1$) potentials ($V \approx 0.16$ in both cases), it becomes significantly lower ($V = 0.077$) at $\varepsilon = 0.25$, reducing (though not eliminating) the first velocity gap. This suggests that existence and stability of low-velocity traveling wave solutions are strongly influenced by the nonlinearity of the substrate potential and not only by the width of the spinodal region (which only slightly increases with ε). Recall that in the case of the biquadratic potential ($\varepsilon = \delta = 0$) the lowest nonzero velocity in the Riemann simulation was $V = 0.424$, and only the higher-velocity kinetic branch contained stable solutions.

VIII. CONCLUDING REMARKS

We studied the effect of nonlinearity of the elastic interaction potential on the motion of a twinning dislocation in the framework of FK model. Using a piecewise quadratic interaction potential potential with non-degenerate spinodal region, we showed that the width of the region has a significant effect on the kinetics of the dislocation and the existence and stability of steady motion at low velocities. As the width of the spinodal region is increased, the lowest propagation speed becomes smaller and eventually slowly moving dislocations that emit waves in both directions become admissible. We presented numerical simulations that

suggest stability of some of the obtained solutions and conjectured that a necessary condition for stability is that the solution is located on an increasing part of the kinetic relation. Both numerical results and analytical calculations show the existence of velocity gaps in which there is no steady motion. Depending on the width of the spinodal region, these gaps can be much narrower than predicted by the biquadratic model. Numerical simulations with smooth potentials show that the gaps persist but may be further reduced by a stronger nonlinearity. We conclude that the velocity gaps are a generic feature of the underdamped discrete model. The gaps are completely eliminated only when unrealistically high internal damping is included into the model.[10,20]

Although we presented our results in the context of a twinning dislocation motion, the main conclusions apply more generally to a variety of physical and biological processes that can be described by the FK model or related higher-dimensional lattice models. To extend our calculations to a periodic potential one needs to impose additional constraints on the values of the displacement in each well.[20] This will yield an upper bound for velocity beyond which the constructed solutions are no longer valid because the large amplitude of oscillations behind the front violates the constraints. However, the low-velocity behavior of solutions connecting two neighboring wells will remain the same. Of course, a periodic potential also makes possible solutions that connect non-neighboring wells (e.g. 4π-kinks[13]), and such solutions are clearly beyond the scope of this work.

It remains unclear whether there are any periodic attractors (not of the traveling wave form) with average velocity inside one of the velocity gaps. If such solutions do exist and are stable, the generic piecewise constant initial conditions we used do not appear to be in their basin of attraction.

Acknowledgments

This work was supported by the NSF Grant DMS-0443928. We thank Phoebus Rosakis for inspiring discussions.

---

* Electronic address: `aav4@pitt.edu`

[1] P. Müllner, V. A. Chernenko, and G. Kostorz, Scripta Materialia **49**, 129 (2003).

[2] D. Bray and J. Howe, Metall. Mat. Trans. A **27A**, 3362 (1996).

[3] J. P. Hirth, Metall. Mat. Trans. A **25A**, 1885 (1994).

[4] J. P. Hirth and J. Lothe, *Theory of dislocations* (John Wiley and Sons, 1982).

[5] R. Abeyaratne and S. Vedantam, J. Mech. Phys. Solids **51**, 1675 (2003).

[6] W. Atkinson and N. Cabrera, Phys. Rev. A **138**, 763 (1965).

[7] A. Carpio and L. L. Bonilla, Phys. Rev. B **71**, 134105 (2005).

[8] V. Celli and N. Flytzanis, J. Appl. Phys. **41**, 4443 (1970).

[9] S. Ishioka, J. Phys. Soc. Jpn. **30**, 323 (1971).

[10] S. Ishioka, J. Phys. Soc. Jpn. **34**, 462 (1973).

[11] O. Kresse and L. Truskinovsky, J. Mech. Phys. Solids **51**, 1305 (2003).

[12] N. Flytzanis, S. Crowley, and V. Celli, J. Phys. Chem. Solids **38**, 539 (1977).

[13] M. Peyrard and M. D. Kruskal, Physica D **14**, 88 (1984).

[14] R. Boesch, C. R. Willis, and M. El-Batanouny, Phys. Rev. B **40**, 2284 (1989).

[15] O. M. Braun and Y. S. Kivshar, *The Frenkel-Kontorova model: concepts, methods and applications*, Texts and monographs in physics (Springer-Verlag, Berlin Heidelberg, 2004).

[16] J. Frenkel and T. Kontorova, Proc. Z. Sowj. **13**, 1 (1938).

[17] A. Carpio and L. L. Bonilla, Phys. Rev. E **67**, 056621 (2003).

[18] A. Vainchtein (2009), submitted, preprint available at www.mathematics.pitt.edu/documents/spinodal.pdf.

[19] J. H. Weiner and W. T. Sanders, Phys. Rev. **134**, 1007 (1964).

[20] O. Kresse, Ph.D. thesis, University of Minnesota, Minneapolis, MN (2002).

[21] A. Carpio, Phys. Rev. E **69**, 046601 (2004).